



Comprehensive Parent–Metabolite PBPK/PD Modeling Insights into Nicotine Replacement Therapy Strategies

Lukas Kovar¹ · Dominik Selzer¹ · Hannah Britz¹ · Neal Benowitz² · Gideon St. Helen² · Yvonne Kohl³ · Robert Bals⁴ · Thorsten Lehr¹ 

Published online: 12 March 2020
© The Author(s) 2020

Abstract

Background Nicotine, the pharmacologically active substance in both tobacco and many electronic cigarette (e-cigarette) liquids, is responsible for the addiction that sustains cigarette smoking. With 8 million deaths worldwide annually, smoking remains one of the major causes of disability and premature death. However, nicotine also plays an important role in smoking cessation strategies.

Objectives The aim of this study was to develop a comprehensive, whole-body, physiologically based pharmacokinetic/pharmacodynamic (PBPK/PD) model of nicotine and its major metabolite cotinine, covering various routes of nicotine administration, and to simulate nicotine brain tissue concentrations after the use of combustible cigarettes, e-cigarettes, nicotine gums, and nicotine patches.

Methods A parent–metabolite, PBPK/PD model of nicotine for a non-smoking and a smoking population was developed using 91 plasma and brain tissue concentration–time profiles and 11 heart rate profiles. Among others, cytochrome P450 (CYP) 2A6 and 2B6 enzymes were implemented, including kinetics for CYP2A6 poor metabolizers.

Results The model is able to precisely describe and predict both nicotine plasma and brain tissue concentrations, cotinine plasma concentrations, and heart rate profiles. 100% of the predicted area under the concentration–time curve (AUC) and maximum concentration (C_{\max}) values meet the twofold acceptance criterion with overall geometric mean fold errors of 1.12 and 1.15, respectively. The administration of combustible cigarettes, e-cigarettes, nicotine patches, and nicotine gums was successfully implemented in the model and used to identify differences in steady-state nicotine brain tissue concentration patterns.

Conclusions Our PBPK/PD model may be helpful in further investigations of nicotine dependence and smoking cessation strategies. As the model represents the first nicotine PBPK/PD model predicting nicotine concentration and heart rate profiles after the use of e-cigarettes, it could also contribute to a better understanding of the recent increase in youth e-cigarette use.

Electronic supplementary material The online version of this article (<https://doi.org/10.1007/s40262-020-00880-4>) contains supplementary material, which is available to authorized users.

✉ Thorsten Lehr
thorsten.lehr@mx.uni-saarland.de

¹ Clinical Pharmacy, Saarland University, Campus C2 2, 66123 Saarbrücken, Germany

² Department of Medicine, University of California, San Francisco, CA, USA

³ Fraunhofer Institute for Biomedical Engineering IBMT, Sulzbach, Germany

⁴ Department of Internal Medicine V, Saarland University, Homburg, Germany

Key Points

A whole-body, parent–metabolite, physiologically based pharmacokinetic/pharmacodynamic model of nicotine was built and evaluated for the prediction of nicotine and cotinine plasma concentrations, nicotine brain tissue concentrations, and heart rate profiles after nicotine intake. The model was able to quantify the contribution of the elimination pathways of nicotine being metabolized to cotinine and renally excreted.

The model was applied to simulate nicotine brain tissue concentration patterns after smoking cigarettes, the administration of nicotine gums (2 mg and 4 mg), and a transdermal nicotine patch.

This study demonstrates the applicability of physiologically based pharmacokinetic modeling to investigate brain tissue concentrations and to successfully integrate many different routes of administration in one model: intravenous, pulmonary (combustible cigarettes and electronic cigarettes), oral (solutions, capsules, and nicotine gums), and transdermal (nicotine patches). Moreover, it represents the first nicotine physiologically based pharmacokinetic model that predicts nicotine plasma concentration and heart rate profiles after the use of electronic cigarettes.

1 Introduction

Tobacco use is now the leading single preventable cause of death worldwide, causing 8 million deaths per year mainly from cardiovascular disease, cancer, and pulmonary disease, according to the latest World Health Organization (WHO) report on the global tobacco epidemic in 2019 [1]. Moreover, despite more than 70% of smokers wanting to quit and 40% attempting to do so each year, only about 5% are successful [2]. The highly addictive nature of tobacco is caused mainly by the pharmacologically active nicotine and often impedes smoking withdrawal [3]. The low quit rates highlight the tremendous need for more successful smoking cessation strategies. In addition, health risks of electronic cigarettes (e-cigarettes) are currently a topic of considerable debate. Preliminary data from the US National Youth Tobacco Survey indicate a further rise in the rates of e-cigarettes use by youth, where the addictive properties of nicotine also play an important role, and which was recently called an “epidemic of youth use of electronic nicotine delivery system products” by the US Food and Drug Administration [4]. While

e-cigarettes assist smoking cessation for some smokers, the escalating rates raise concerns about addicting a generation of young people to nicotine, with the long-term safety of e-cigarettes still unknown [5]. A better understanding of differences in the pharmacokinetics (PK) of nicotine, including nicotine exposure in the brain after different routes of administration, may enhance the understanding of nicotine addiction with the use of different nicotine delivery products and inform more successful treatment interventions.

While nicotine plays only a minor direct role in causing smoking-induced diseases, addiction to nicotine is the proximate cause of these diseases [3]. When nicotine is inhaled, it is rapidly absorbed into the pulmonary venous circulation, and quickly reaches the brain tissue through arterial circulation. There, it immediately induces pharmacodynamic (PD) effects including the release of dopamine in the mesolimbic area, a key step in causing nicotine addiction [6]. For smokers who intend to quit smoking, nicotine maintenance with nicotine replacement therapies (NRTs) such as nicotine gums or transdermal patches can help reduce smoking rates and facilitate smoking cessation [7, 8]. Although NRTs try to imitate the nicotine exposure of smoking, nicotine appearance in the venous blood is slower and peak concentrations are lower with the use of NRTs, compared with smoking combustible cigarettes [9, 10]. Data on nicotine brain tissue concentrations are scarce and typically complex in nature [11]. Nevertheless, it would be of great interest to also compare differences in nicotine exposure in brain tissue after various routes of nicotine administration.

Genetic factors account for about 30% of the variance in risk for failed smoking cessation [12] and pharmacogenetic testing has shown the potential to optimize smoking cessation therapies [13, 14]. Thus, cytochrome P450 (CYP) enzymes, which are involved in metabolizing nicotine, are of significant interest when investigating nicotine pharmacokinetics. For example, poor metabolizers (PM) of CYP2A6, which is predominantly responsible for nicotine metabolism [15], have a lower risk of developing nicotine dependence and less severe nicotine withdrawal symptoms than normal metabolizers (NM) [16].

In addition to its addictive effects on the brain, nicotine acts as a sympathomimetic drug, releasing catecholamines and thereby inducing peripheral PD effects such as an increase in heart rate [17]. Changes in heart rate represent a surrogate measure for general pharmacological actions of nicotine. Cotinine is widely used as a biomarker for the use of tobacco, as a quantitative marker for exposures to nicotine, and as a measure of compliance with treatments of smoking cessation, owing to its long half-life compared with nicotine (~16 h vs ~2 h) and consequently, fairly stable cotinine plasma concentrations in regular daily smokers [6, 18].

Physiologically based pharmacokinetic (PBPK) modeling offers a solution to tackle these complexities of nicotine

pharmacokinetics and pharmacodynamics and provides the opportunity to characterize and predict drug exposure in a specific organ or tissue [19]. The aims of this study were (1) to develop a whole-body PBPK/PD model of nicotine and its major metabolite cotinine, covering various routes of administration (i.e., intravenous, oral, transdermal, and pulmonary) including the PK/PD relationship in heart rate changes, (2) to provide a comprehensive publicly available model for further investigations and applications, which may contribute to the WHO's goal of combating the tobacco epidemic and to stop the persistent rise in youth e-cigarette use [1, 4], and finally, (3) to apply the model to investigate differences in brain concentrations between pulmonary administration of nicotine (combustible cigarettes, e-cigarettes) and NRTs.

2 Methods

2.1 Software

The PBPK/PD modeling and simulation was performed using PK-Sim[®] and MoBi[®] (version 8.0, part of the Open Systems Pharmacology [OSP] suite, <https://www.open-systems-pharmacology.org>). Model input parameter optimization was accomplished using the Monte Carlo algorithm. Clinical data were digitized using GetData Graph Digitizer version 2.26.0.20 (S. Fedorov). PK parameter analyses and graphics were compiled with the R programming language version 3.6.0 (R Foundation for Statistical Computing, Vienna, Austria).

2.2 Physiologically Based Pharmacokinetic/Pharmacodynamic (PBPK/PD) Parent–Metabolite Model Building

For PBPK/PD model building, an extensive literature search was performed to collect information on physicochemical properties, liberation, absorption, distribution, metabolism, and excretion (LADME) processes and clinical studies of intravenous, oral, pulmonary, and transdermal administration of nicotine and intravenous administration of cotinine in single- and multiple-dose regimens. Plasma concentration–time profiles, a brain tissue concentration–time profile, fractions of nicotine and cotinine doses excreted unchanged to urine, and heart rate profiles were digitized from 34 clinical studies with 75 different treatment blocks and 891 patients and split into an internal training ($n=26$ profiles) and an external test ($n=76$ profiles) dataset (for detailed information on clinical studies, see Tables S2.6.1–S2.6.3 of the Electronic Supplementary Material [ESM]). The internal training dataset was used for model building and together with the external test dataset, for model evaluation. The training dataset was selected so as to inform all physiological

processes implemented in the model (e.g., contribution of the CYP2B6 elimination pathway, estimation of urinary excretion).

Hence, for cotinine PBPK model building, three plasma profiles of cotinine administered intravenously were used, which covered a broad dosing range and included information on urinary excretion of cotinine. For the nicotine PBPK model building, plasma profiles of non-smokers and smokers after intravenous administration were included in the training dataset, with a broad dosing range, including studies with cotinine metabolite data, information on the fraction of nicotine excreted unchanged to urine, and the fraction of nicotine metabolized to cotinine. Moreover, a study with plasma concentrations of CYP2A6 poor metabolizers and a study with brain tissue concentrations after nicotine intake were included in the training dataset, to inform model input parameters for CYP2B6 and brain transporters. For the PD heart rate model, three studies with intravenous administration were used for model training, which covered the largest timeframe of heart rate measurements and the highest nicotine peak plasma concentrations. Values for model input parameters that could not be adequately obtained from the literature were estimated by fitting first the cotinine model and subsequently the nicotine model to the training dataset.

The parent–metabolite PBPK/PD model was derived using a stepwise approach. Initially, a cotinine model was developed based on cotinine intravenous training data from healthy non-smoking volunteers. Second, the cotinine model was complemented by a comprehensive PBPK model of the parent compound nicotine, including intravenous, oral, and pulmonary administration of nicotine, using the internal dataset for model training. Third, the oral route of administration for nicotine gums and a transdermal model were established and added to the parent–metabolite PBPK model. Fourth, a modified heart rate–tolerance PD model based on a recently published tolerance model, including circadian rhythm [20] was incorporated into the PBPK model to describe the positive chronotropic effect of nicotine. Finally, the resulting PBPK/PD model was evaluated and used to simulate brain tissue concentration patterns after nicotine administration through different routes.

Distribution and elimination processes including CYP enzymes and transporters were implemented according to the literature [15, 21–23]. For the nicotine model, these are (1) metabolism of nicotine to its major metabolite cotinine through CYP2A6 and CYP2B6, (2) an unspecific hepatic clearance being responsible for the remaining hepatic metabolism of nicotine including metabolism via uridine 5'-diphospho-glucuronosyltransferase 2B10 (UGT2B10) and flavin-containing monooxygenase 3 (FMO3), and (3) two transporters for the influx and efflux of nicotine across the blood–brain barrier (BBB). For cotinine, an unspecific hepatic clearance was implemented. Additionally, renal

excretion through glomerular filtration was implemented as an elimination pathway for both compounds, as they are subject to glomerular filtration under physiological conditions [15, 24]. Reported differences in nicotine clearance between smokers and non-smokers [25] were addressed by estimating different values for the CYP2A6 catalytic rate constant (k_{cat}).

A PD model was added to the PBPK model to describe the positive chronotropic effect of nicotine [9, 26] based on its PK. The model, which best described the heart rate including the drug effect, was a direct-effect E_{max} model with absolute effect, including a tolerance development based on a recently published heart rate tolerance model [20]. Figure 1 shows a structural overview of the developed PBPK/PD model. The tolerance compartment was implemented to describe the extent of acute tolerance development of the system and its subsequent reduction in the drug effect on heart rate following the administration of nicotine [27]. The appearance of tolerance was set to depend on the concentration of nicotine, which has been shown in the literature [27]. For detailed information on PBPK/PD model building and virtual populations, see Sect. 2 of the ESM.

2.3 PBPK Model of Nicotine Patches, Nicotine Gums, Combustible Cigarettes, and Electronic Cigarettes

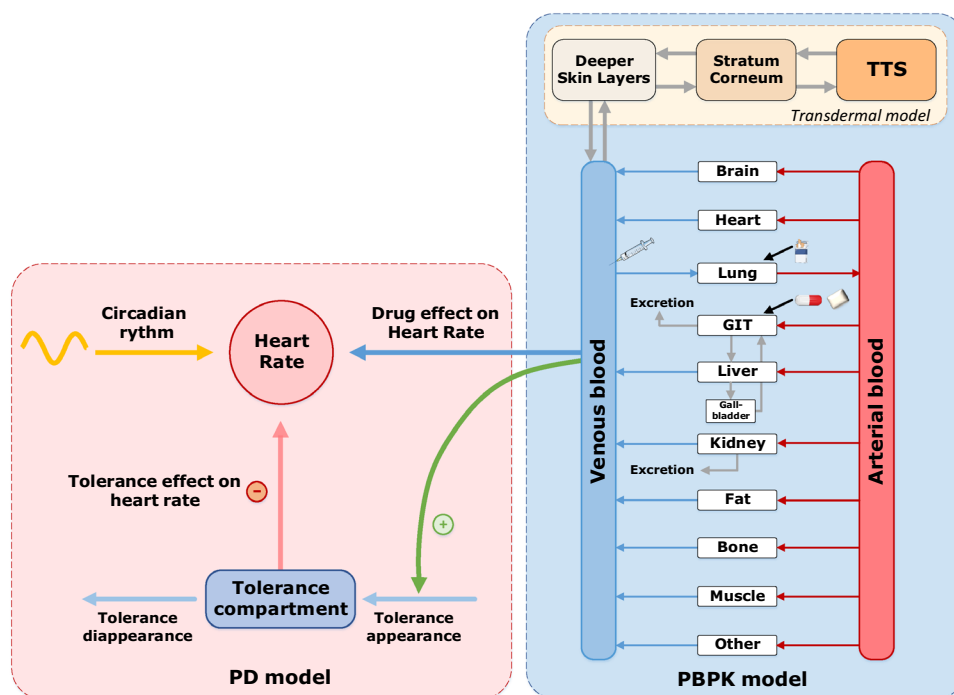
To model and simulate the transdermal application of nicotine with nicotine patches, a transdermal two-compartment skin model was implemented with MoBi[®] and added to the default PBPK model. To model and simulate the

administration of nicotine gums, an oral formulation was used. The corresponding nicotine release was implemented according to a published in vitro release profile of Nicorette[®] chewing gums [28]. A pulmonary route of administration was applied within PK-Sim[®] to model and simulate the inhalation of nicotine with combustible cigarettes and e-cigarettes. Zero-order kinetics were chosen for pulmonary formulations with a duration of the length of smoking, which is supported by the literature [29]. For detailed information see Sects. 2.2–2.4 of the ESM.

2.4 PBPK/PD Model Evaluation

All the 102 nicotine and cotinine concentration–time profiles and heart rate profiles observed of the training and test datasets were compared to predicted profiles. Virtual populations of 100 individuals for each study were established according to the population demographics of the respective simulated study. Population predictions were plotted as geometric mean with geometric standard deviation. Visual descriptive (training dataset) and predictive (test dataset) performances of the PBPK/PD model are shown in Sect. 3 and in detail in Sects. 3.1–3.6 and 3.11 of the ESM. Model performance was also evaluated by comparing predicted plasma concentrations with their respective values observed in goodness-of-fit plots. Additionally, the predicted vs observed area under the concentration–time curve from the first to the last data point (AUC_{last}) and maximum concentration (C_{max}) values were compared in goodness-of-fit plots. The sensitivity of the final PBPK model to single parameter changes (local

Fig. 1 Structural overview of the developed physiologically based pharmacokinetic/pharmacodynamic (PBPK/PD) model for the intravenous, oral, transdermal, and pulmonary administration of nicotine. Boxes indicate compartments, solid lines denote in-/out-flows, dashed lines indicate relationships. *GIT* gastrointestinal tract, *TTS* transdermal therapeutic system



sensitivity analysis) was investigated with PK-Sim[®]. Further, two quantitative performance measures were calculated: the mean relative deviation (MRD) of the predicted plasma concentrations for each plasma profile and the geometric mean fold errors (GMFE) of AUC_{last} and C_{max} , respectively (see Sects. 3.8–3.10 of the ESM).

3 Results

3.1 PBPK Model Building and Evaluation

The whole-body PBPK model of nicotine and cotinine precisely describes and predicts plasma concentration–time profiles following intravenous, oral, transdermal, and pulmonary administration and data on brain tissue concentrations (see Figs. 2, 3, 4, 5). For the building and evaluation of the nicotine parent–metabolite PBPK model, 90 plasma concentration–time profiles including 18 cotinine metabolite profiles, a brain tissue concentration–time profile, six

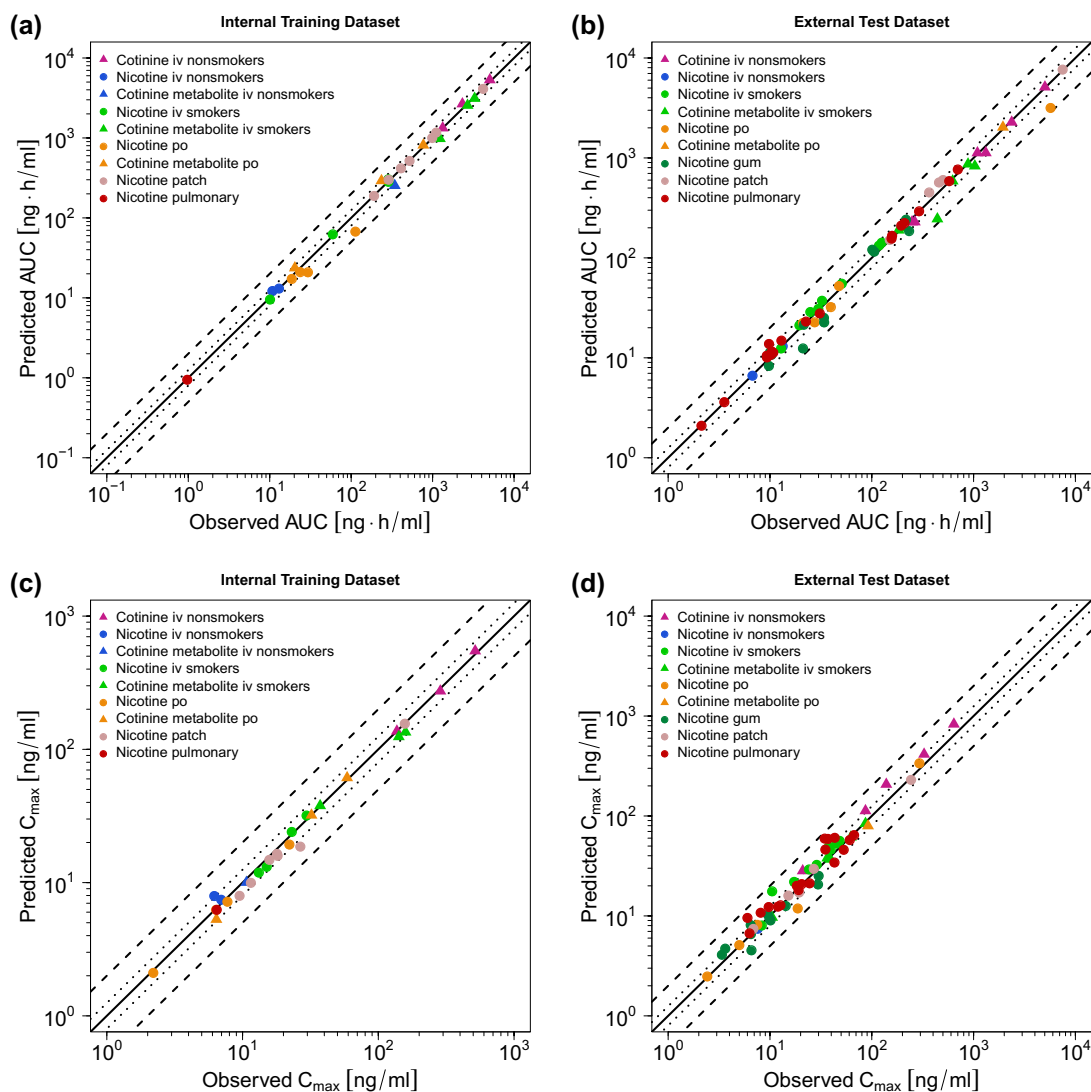


Fig. 2 Predicted vs observed nicotine and cotinine area under the concentration–time curve from the first to the last data point (AUC) [a, b] and maximum concentration (C_{max}) [c, d] values of the internal training and the external test dataset. Each symbol represents the AUC or C_{max} of a single concentration–time profile (circles: nicotine,

triangles: cotinine metabolite and cotinine intravenous [iv]). The black solid lines mark the lines of identity. Black dotted lines indicate a 1.25-fold deviation, black dashed lines indicate a twofold deviation. *Patch* transdermal therapeutic system (nicotine patch), *po* oral

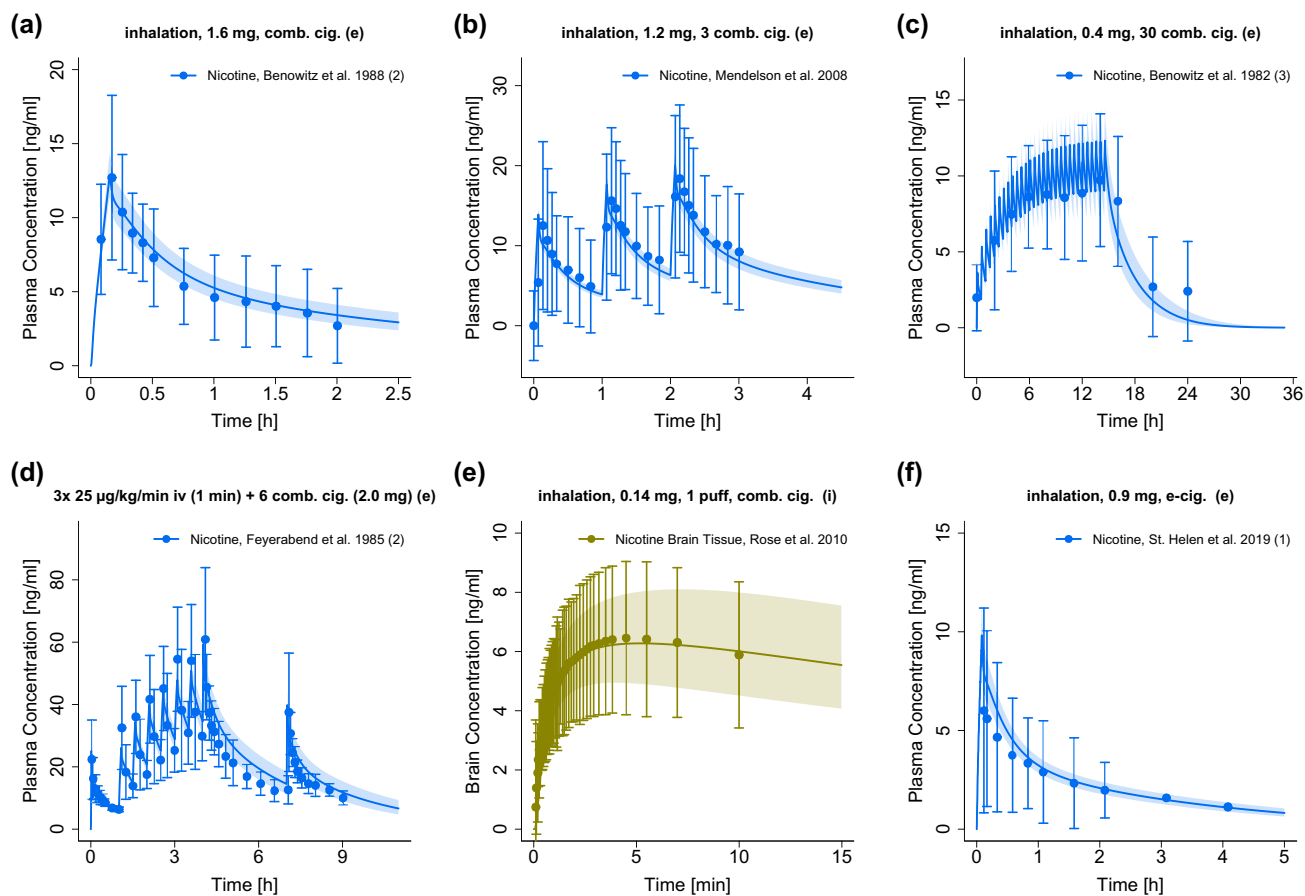


Fig. 3 Nicotine predicted and observed plasma (blue) and brain tissue (gold) concentration–time profiles after administration of combustible cigarettes (with estimated pulmonary nicotine exposure for plasma simulations) and electronic cigarettes (e-cig.). Population simulation ($n=100$) geometric means are shown as lines; the shaded areas represent the predicted population geometric standard deviations (SDs). Observed data are shown as filled circles \pm SD. (i): selection of

internal training dataset, (e): selection of external test dataset. References with numbers in parentheses link to a specific observed dataset described in the study table with detailed information about dosing regimens (Tables S2.6.1 and S2.8.2 of the ESM). Predicted and observed area under the concentration–time curve (AUC) and maximum concentration (C_{\max}) values are compared in Table S3.8.2 of the ESM. *comb. cig.* combustible cigarette, *iv* intravenous [9, 11, 70–73]

studies on the fraction of nicotine and cotinine excreted unchanged to urine, and one study depicting the fraction of nicotine metabolized to cotinine were used. Drug-dependent parameters of the final parent–metabolite PBPK model are depicted in Table 1. A study overview including key metrics and a detailed description of the PBPK model are listed in Sect. 2 of the ESM.

The good descriptive and predictive model performance is comprehensively demonstrated. Visual comparisons of predicted to observed plasma concentration–time profiles are depicted in Figs. 3, 4, 5 (selection of internal and external datasets for each route of administration) and in detail in Sects. 3.1–3.6 of the ESM (all studies, linear and semilogarithmic plots). The predictions of plasma concentration–time trajectories for all routes of administration are in close agreement with observed plasma concentration data. Moreover, goodness-of-fit plots of predicted to observed AUC_{last} and C_{\max} are shown in Fig. 2 and for each route of administration

separately in Sects. 3.1–3.6 of the ESM together with goodness-of-fit plots of observed vs predicted plasma concentrations. In summary, 100% of both the predicted AUC_{last} and C_{\max} values appear to be within the twofold acceptance criterion. The GMFE values for the nicotine PBPK model are 1.11 and 1.17 for AUC_{last} and C_{\max} , respectively, and 1.14 and 1.11 for the cotinine model. Overall MRD for the nicotine and cotinine PBPK model are 1.44 and 1.77, respectively. Detailed results on GMFE and MRD values calculated for all studies are given in Sect. 3.8 of the ESM and the results of the sensitivity analysis are shown in Sect. 3.10 of the ESM.

Nicotine is mainly metabolized through CYP2A6. However, in CYP2A6 PMs, when people lack CYP2A6 metabolism and cotinine production diminishes (CYP2A6- k_{cat} of 0), CYP2B6 is responsible for a modest nicotine conversion to cotinine [15, 22]. A CYP2A6 PM plasma concentration–time profile was included in the training dataset to

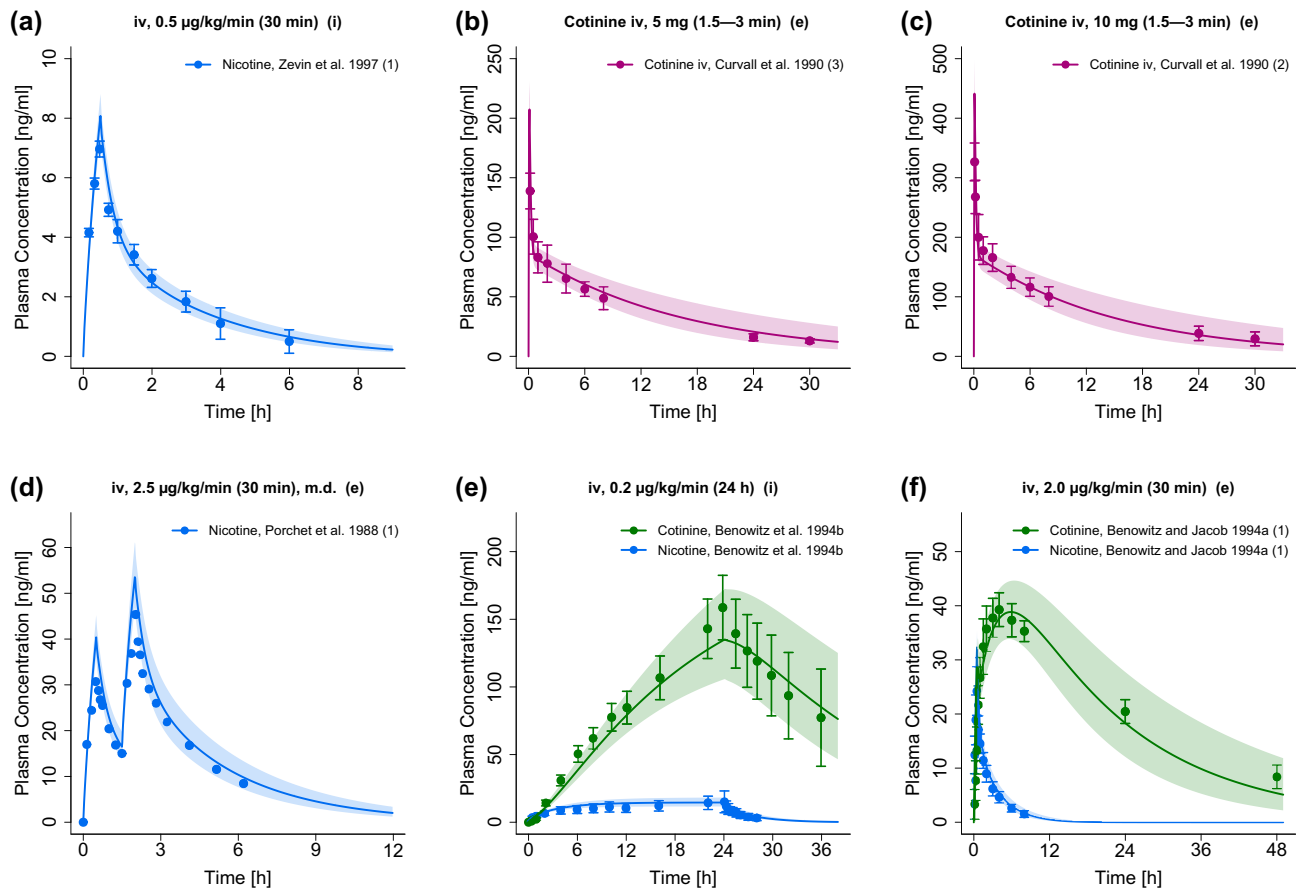


Fig. 4 Nicotine (blue) and cotinine (purple if administered intravenously, green if metabolite) predicted and observed plasma concentration–time profiles after intravenous administration. **a–c** Non-smokers, **d–f**: smokers. Population simulation ($n=100$) geometric means are shown as lines; the shaded areas represent the predicted population geometric standard deviations (SDs). Observed data are shown as filled circles, if available \pm SD. (i): selection of internal training

estimate CYP2B6 metabolism in the model and to describe nicotine plasma concentrations in CYP2A6 PMs (see Fig. 5d) [40]. Additionally, nicotine clearance in smokers appears to be about 15% lower, compared with non-smokers [25]. To account for this difference, CYP2A6- k_{cat} was estimated separately for the smoker subpopulation, leading to a lower k_{cat} in comparison to the non-smoker subpopulation (see Table 1). For detailed information including drug-, system-, and formulation-dependent model parameters, see Sect. 2.1 of the ESM and Tables S2.7.1, S2.8.1–2.8.3, and S2.10.1 of the ESM.

The resulting PBPK model predicts a fraction of nicotine metabolized to cotinine of about 75%, which perfectly aligns with literature reports (70–80%) [15, 22, 23]. Moreover, predicted bioavailabilities after oral (~35%) and pulmonary (~85%) administration of nicotine are in concordance with the literature (20–45% and 80–90%, respectively) [9, 15, 46].

dataset, (e): selection of external test dataset. References with numbers in parentheses link to a specific observed dataset described in the study table with detailed information about dosing regimens (Tables S2.6.1 and S2.6.2 of the ESM). Predicted and observed area under the plasma concentration–time curve (AUC) and maximum plasma concentration (C_{max}) values are compared in Table S3.8.2. of the ESM. *iv* intravenous [22, 27, 74–76]

As the published literature suggests, the influx and efflux of nicotine over the BBB play an important role in the characteristics of nicotine brain tissue concentrations [21]. As a result, an influx and an efflux transporter with Michaelis–Menten kinetics were implemented in the BBB, which led to a precise description of experimental nicotine brain tissue concentrations after a puff of a combustible cigarette (see Fig. 3e) [11].

It is known that machine smoking yields of combustible cigarettes are not equivalent to human measures of nicotine uptake [47, 48]. Hence, when machine smoking yields are used as nicotine doses for simulation of plasma concentrations, the model underpredicts observed data for low machine smoking yields and overpredicts observed data for high machine smoking yields (see Fig. S3.6.1 of the ESM). Therefore, pulmonary nicotine exposure for combustible cigarettes was estimated additionally as described in Sect. 2.4 of the ESM (mean deviation to

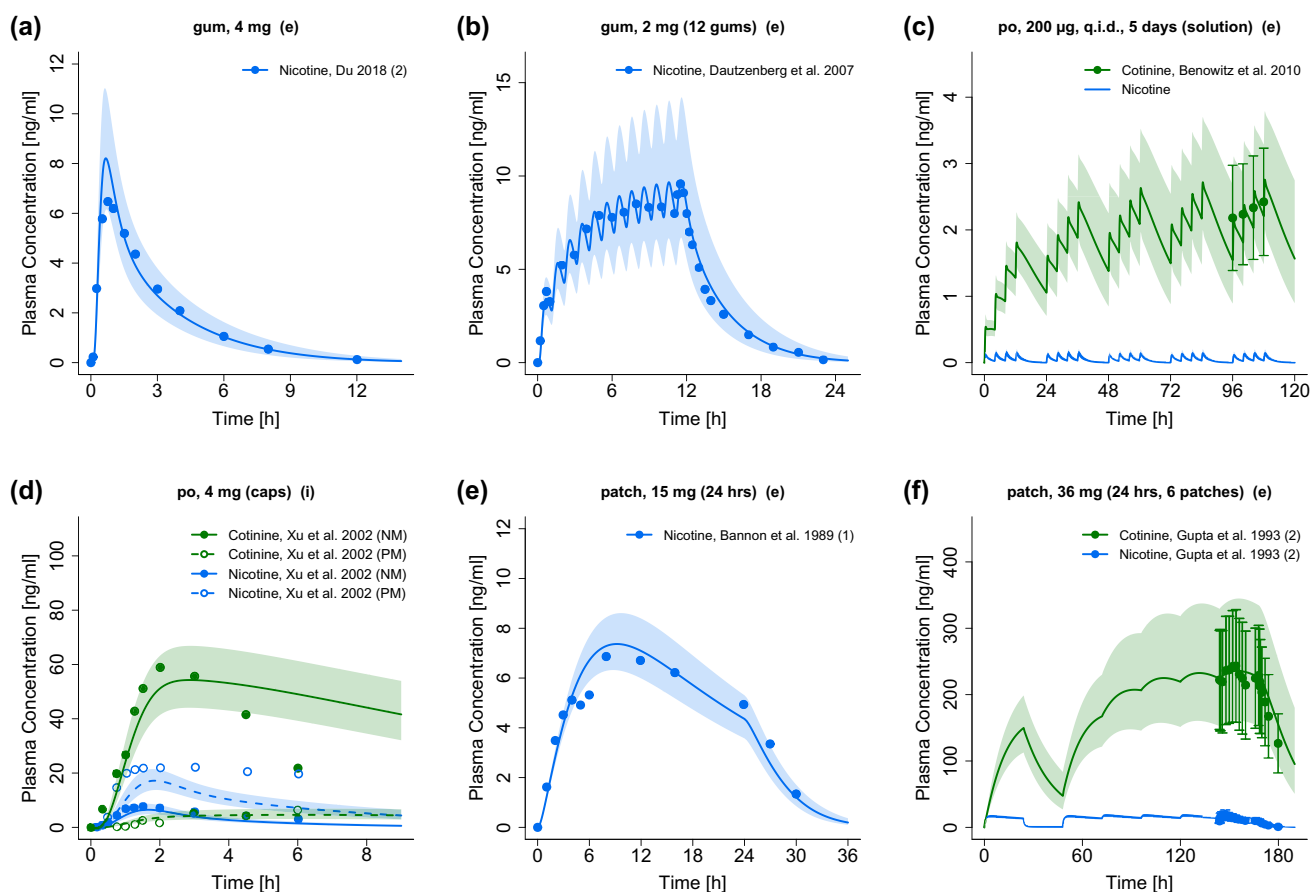


Fig. 5 Nicotine (blue) and cotinine metabolite (green) predicted and observed plasma concentration–time profiles after oral (gum, solution, capsule) and transdermal administration. Population simulation ($n=100$) geometric means are shown as lines; the shaded areas represent the predicted population geometric standard deviations (SDs). Observed data are shown as circles, if available \pm SD. (i): selection of internal training dataset, (e): selection of external test dataset. References with numbers in parentheses link to a specific observed data-

set described in the study table with detailed information about dosing regimens (Tables S2.6.1 and S2.8.3 of the ESM). Predicted and observed area under the plasma concentration–time curve (AUC) and maximum plasma concentration (C_{max}) values are compared in Table S3.8.2. of the ESM. *caps* capsule, *NM* normal metabolizer, *patch* transdermal therapeutic system (nicotine patch), *PM* poor metabolizer, *po* oral, *q.i.d.* four times daily [18, 40, 62, 77–79]

machine smoked nicotine yields of 31%), leading to the precise predictions of plasma profiles observed (see Fig. 3 and Fig. S3.5.1 of the ESM).

For the administration of nicotine through transdermal therapeutic systems (TTS), the default PK-Sim[®] PBPK model was expanded with a two-compartment skin model, which consists of the lipophilic stratum corneum and the hydrophilic deeper skin layer routes. The resulting model successfully describes and predicts plasma profiles after single and multiple doses of nicotine patches (see Fig. 5e, f and Sect. 3.4 of the ESM). The model was also able to predict nicotine plasma profiles during the use of nicotine gums in single- and multiple-dose studies (see Fig. 5a, b and Sect. 3.3 of the ESM) and cotinine steady-state plasma concentrations observed in several studies (see Fig. 5c, f and Sect. 3.3 of the ESM) [18].

3.2 Brain Concentrations after Different Routes of Administration

The model was used to simulate steady-state brain tissue concentrations throughout a day when smoking combustible cigarettes or e-cigarettes (16 cigarettes during 16 h), administering nicotine gums (16 gums during 16 h), or applying a nicotine patch (for 24 h). Simulations and results of the comparison of area under the brain tissue concentration–time curves, maximum brain tissue concentrations, and peak-trough differences for each type of nicotine administration are depicted in Fig. 6.

Table 1 Drug-dependent and pharmacodynamic (PD) parameters of the final parent–metabolite physiologically based pharmacokinetic/pharmacodynamic (PBPK/PD) model

Parameter	Unit	Nicotine model		Cotinine model		Description ^a
		Value used in simulation	Literature value [Ref]	Value used in simulation	Literature value [Ref]	
PBPK model						
MW	g/mol	162.2	162.2 [30] ^b	176.2	176.2 [30] ^c	Molecular weight
pK _{a1}		8.1 (basic)	8.1 [31]	4.5 (basic)	4.5 [32]	Acid dissociation constant 1
pK _{a2}		3.3 (basic)	3.3 [31]			Acid dissociation constant 2
log <i>P</i>		1.6	1.2, 1.4 [31, 33]	−0.1 ^f	0.21 [30] ^c	Lipophilicity
Solubility (pH)	mg/mL	93.3 (7.0)	93.3 (7.0) [30] ^b	117.0 (7.0)	117.0 (7.0) [30] ^c	Solubility
<i>f</i> _u	%	95.1	80.0–95.1 [34]	97.4	97.4 [35]	Fraction unbound (plasma)
CYP2A6 <i>K</i> _M	μmol/L	29.4 ^f	11.0, 32.0, 33.0, 144.0 [36–39]			CYP2A6 Michaelis–Menten constant
CYP2A6-NM <i>k</i> _{cat} (non-smokers)	1/min	12.0 ^f	–			CYP2A6-NM catalytic rate constant for non-smokers
CYP2A6-NM <i>k</i> _{cat} (smokers)	1/min	10.5 ^f	–			CYP2A6-NM catalytic rate constant for smokers
CYP2A6-PM <i>k</i> _{cat}	1/min	0.0	0 [40]			CYP2A6-PM catalytic rate constant
CYP2B6 <i>K</i> _M	μmol/L	820.0	820.0 [41]			CYP2B6 Michaelis–Menten constant
CYP2B6 <i>k</i> _{cat}	1/min	16.0 ^f	–			CYP2B6 catalytic rate constant
BBB-transporter _{in} <i>K</i> _M	μmol/L	92.4	92.4 [21]			BBB-transporter _{in} Michaelis–Menten constant
BBB-transporter _{in} <i>k</i> _{cat}	1/s	5.3E+03 ^f	–			BBB-transporter _{in} catalytic rate constant
BBB-transporter _{out} <i>K</i> _M	μmol/L	7.0E−05 ^f	–			BBB-transporter _{out} Michaelis–Menten constant
BBB-transporter _{out} <i>k</i> _{cat}	1/s	0.4 ^f	–			BBB-transporter _{out} catalytic rate constant
GFR fraction		1.0	–	6.0E−02 ^f	–	Fraction of GFR used for passive elimination by the kidney
Unspecific hepatic clearance	1/min	0.3 ^f	–	2.0E−02 ^f	–	Elimination from plasma (first-order process in the liver)
Calculation method of partition coefficients		Rodgers and Rowland [42–44]		PK-Sim [®] standard [45] ^d		Organ-plasma partition coefficients
Calculation method of cell permeabilities		PK-Sim [®] standard [45] ^d		PK-Sim [®] standard [45] ^d		Permeation across cell membranes
PD model^c						
<i>E</i> _{max}	bpm	111.6 ^f	–			Maximum possible heart rate elevation without tolerance

Table 1 (continued)

Parameter	Unit	Nicotine model		Cotinine model		Description ^a
		Value used in simulation	Literature value [Ref]	Value used in simulation	Literature value [Ref]	
EC ₅₀	μmol/L	0.21 ^f	–			Concentration at half-maximum elevation
<i>h</i>		1.3 ^f	–			Hill coefficient
tol _{in}	1/h	15.3 ^f	–			Tolerance appearance rate
tol _{out}	1/h	0.2 ^f	–			Tolerance disappearance rate
tol ₅₀	μmol/L	0.07 ^f	–			Scaling parameter for tolerance
amp	%	6.3	6.3 [20]			Circadian amplitude
γ		0.4 ^f	–			Non-linearity parameter

BBB blood–brain barrier, *bpm* beats/min, *CYP* cytochrome P450, *GFR* glomerular filtration rate, *k_{cat}* catalytic rate constant, *NM* normal metabolizer, *PM* poor metabolizer, *Ref* reference, – not available

^aDescriptions for PD parameters carried over from [20]

^bDrugBank entry for nicotine. Available from: <https://www.drugbank.ca/drugs/DB00184> [Accessed 21 Oct 2019]

^cDrugBank entry for cotinine. Available from: <https://www.drugbank.ca/metabolites/DBMET00519>. [Accessed 21 Oct 2019]

^dEquations and descriptions of calculations can be found in [45]

^eIndividual heart rate baselines and circadian time shift for different study populations are depicted in Sect. 2.9 of the ESM

^fModel input parameter estimated

3.3 PBPK/PD Model Building and Evaluation

The PBPK model has been augmented with a PD nicotine heart rate model (see Fig. 1). The integrated PBPK/PD model is able to capture the effect of nicotine that leads to heart rate peaks rapidly after intravenous and pulmonary nicotine intake. A total of 11 studies evaluating the effect of nicotine on heart rate were used for PD model building and evaluation. Study details and key metrics are listed in Table S2.6.3 of the ESM. Parameters of the final PBPK/PD model are listed in Table 1. PD model performance for both the internal training and the external test dataset is demonstrated by comparing the population predicted to heart rate profiles observed in Fig. 7 (representative studies) and in detail in Sect. 3.11 of the ESM (all studies).

4 Discussion

The main outcome of this study is the development of a comprehensive parent–metabolite PBPK/PD model of a drug, which is consumed by over 1.1 billion smokers and which is also used in NRTs as an important smoking cessation strategy [1]. The model provides a consistent representation of the nicotine dose–exposure relationship following intravenous, oral, transdermal, and pulmonary administration in non-smoking and smoking populations. It precisely

describes and predicts nicotine and cotinine plasma and nicotine brain tissue concentrations. Thereby, the model is able to quantify the contribution of the elimination pathways of the fraction of nicotine metabolized to cotinine and urinary excretion of both nicotine and cotinine. Further, the PBPK model has been expanded by a heart rate tolerance model, which includes circadian rhythm, describing the positive chronotropic effect of nicotine. Finally, the model was used to identify differences in brain concentrations between pulmonary administration of nicotine (combustible cigarettes, e-cigarettes) and NRTs.

To reduce smoking dependence, exposure to smoke toxicants, and youth e-cigarette use, all of which are critical public health goals [1, 4], it is crucial to have quantitative tools to better understand both smoking behavior and dependence on nicotine. This model represents an opportunity to simulate concentrations of nicotine in blood plasma and brain tissue with requested dosing regimens after four different routes of administration.

Five other PBPK models of nicotine have been developed so far; however, either important routes of administration, a PD heart rate model, comprehensive predictive performance, and/or the inclusion of a large number of clinical studies are missing [49–53]. The models developed by Plowchalk et al. (for rats), Robinson et al., and Yamazaki et al. (for humans) presented simplified implementations of the nicotine ADME processes [49–51]. While Teeguarden et al. stated that their

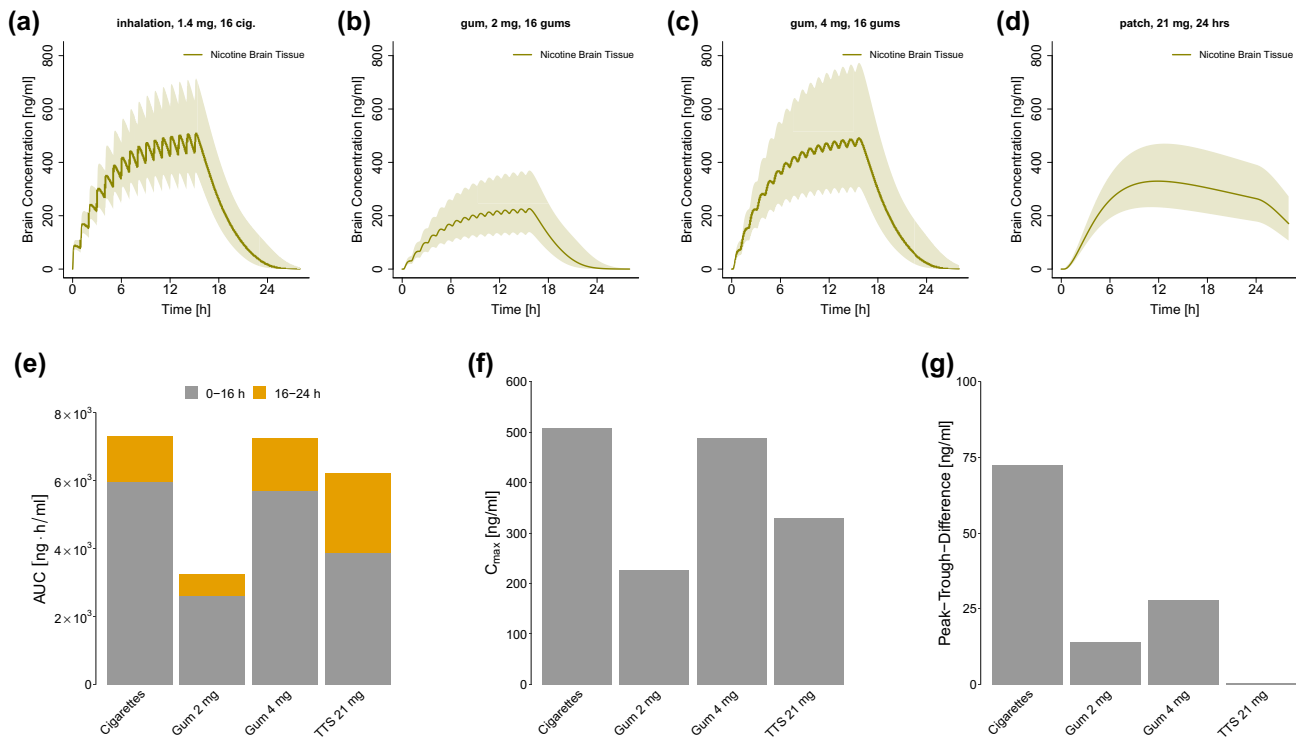


Fig. 6 Simulations of brain tissue concentration–time profiles after pulmonary (16 h), oral (2 mg and 4 mg gums, 16 h), and transdermal (patch, 24 h) administration (**a–d**) and analysis of the area under the brain tissue concentration–time curve (AUC) of nicotine brain tissue concentrations for the first 16 h (gray) and the last 8 h (orange) (**e**), maximum brain tissue concentrations (C_{max}) (**f**), and peak-trough differences in brain tissue concentrations between minimum brain tissue

concentration (C_{min}) and C_{max} in steady state (**g**). Population simulation ($n=100$) geometric means are shown as lines; the shaded areas represent the population geometric standard deviations. Detailed information about dosing regimens, study populations, and parameters used for simulations is given in Tables S2.6.1, S2.7.1, S2.8.1, and S2.8.3 of the ESM. Peak-trough difference is not applicable for the transdermal therapeutic system (nicotine patch). *cig.* cigarettes

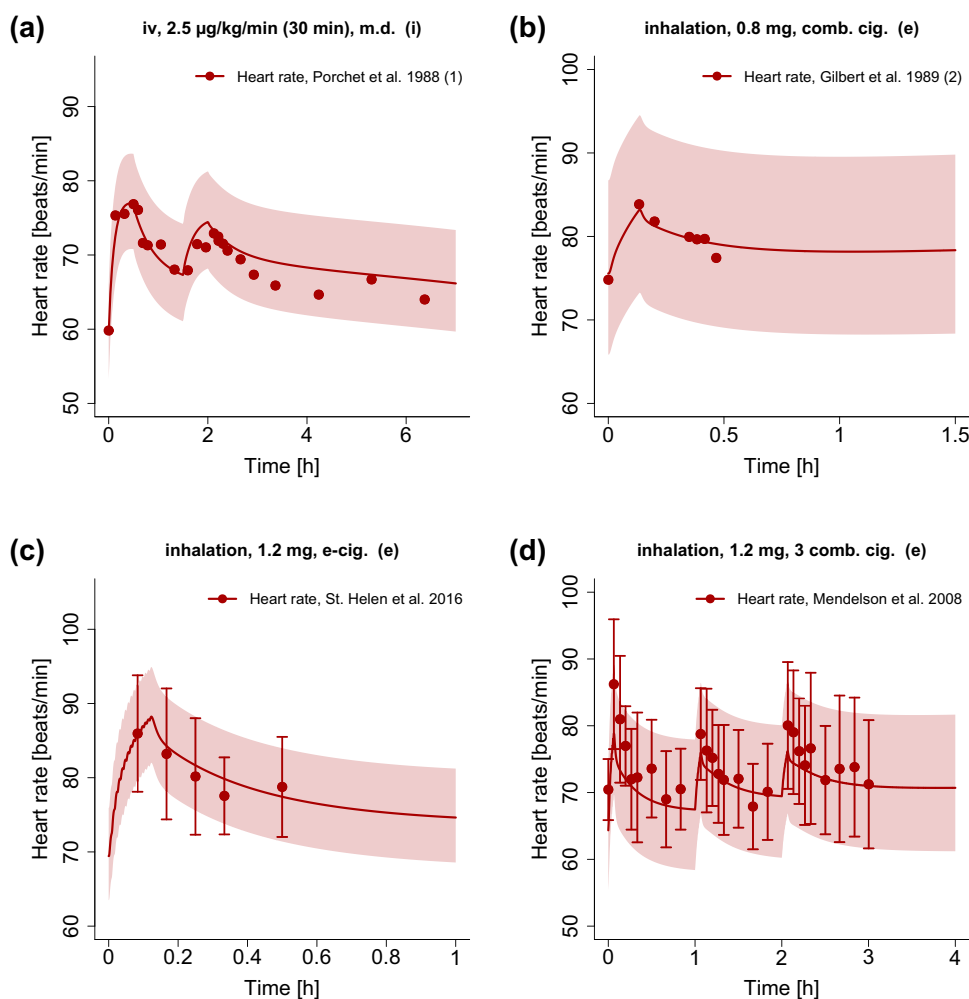
“results should not at this time be considered accurate predictions of outcomes in a population of smokers”, they presented one of the first broad models including several routes of nicotine administration (without a transdermal route) and a PD model [52]. The most current nicotine PBPK/PD model, by Gajewska et al., accurately described heart rate changes after transdermal nicotine intake but struggled to predict heart rate peaks occurring after intravenous nicotine administration and nicotine plasma concentrations after the removal of nicotine patches [53]. While the previously mentioned models provide the information in a condensed form to investigate the models independent of the underlying platform, the presented model relies on the application within the OSP framework. However, all the information can be accessed through the model file, which is publicly available in the OSP repository for application and investigation purposes.

Our PBPK/PD model incorporates comprehensiveness of both the routes of administration (intravenous, transdermal [patches], oral [including gums], and pulmonary [combustible cigarettes and e-cigarettes]) and the number of plasma, brain tissue, and heart rate profiles included

($n=102$) to develop the model. Moreover, this study presents a novel opportunity to simulate nicotine brain tissue concentrations after different routes of administration, based on incorporated information on brain tissue concentrations, in PK-Sim[®] and MoBi[®].

In contrast with already published nicotine PBPK models, this study includes the two most important CYP enzymes for nicotine metabolism, CYP2A6 and CYP2B6, both highly polymorphic, and incorporated differences between CYP2A6 PMs and NMs [15, 40, 54]. This is crucial for the individualization of NRTs to avoid poor response and adverse drug reactions [55, 56], as pharmacogenetic testing has shown the potential to optimize smoking cessation therapies [13, 14]. Because only one plasma–concentration time profile for PMs was available and concentrations were determined only over 6 h, simulations of plasma concentrations may be less accurate over longer time periods. Hence, additional research on the PK of PMs would be of great interest. The enzymatic pathways responsible for nicotine glucuronidation (UGT2B10) and N-oxidation (FMO3) are subsumed under the unspecific hepatic clearance process.

Fig. 7 Predicted and observed heart rate profiles after intravenous (iv) and pulmonary (combustible cigarette [comb. cig.] and electronic cigarette [e-cig.] administration. Population simulation ($n=100$) geometric means are shown as lines; the shaded areas represent the predicted population geometric standard deviations (SDs). Observed data are shown as filled circles, if available \pm SD. (i): selection of internal training dataset, (e): selection of external test dataset. References with numbers in parentheses link to a specific observed dataset described in the study table with detailed information about dosing regimens (Table S2.6.3 of the ESM). *m.d.* multiple dose [27, 70, 80, 81]



Additionally, we present the first nicotine PBPK model that also includes and predicts nicotine concentration–time and heart rate profiles after e-cigarette use. In light of the ongoing discussions on the health risks of e-cigarettes and the fact that more than a quarter of high school students in the USA are current e-cigarette users with the figures still rising, our data might contribute to a better understanding of the persistent increase in youth e-cigarette use by serving as a basis for future studies on nicotine PK-based addiction models [4, 57].

Being widely used as a quantitative marker for exposures to nicotine and as a measure of compliance with treatments for smoking cessation [6, 18], cotinine was also included in the model. The glomerular filtration rate fraction of 0.06 for cotinine, combined with the description of the fraction of cotinine dose excreted unchanged to urine, indicates high tubular reabsorption of cotinine in the kidney. Accurate cotinine metabolite predictions after intravenous, oral (solutions, capsules), and transdermal administration could allow future investigations to perform reverse calculations to arrive at the amount of nicotine intake from cotinine plasma

concentrations with this model. Because no cotinine metabolite data after pulmonary and nicotine gum intake were available, cotinine formation could not be evaluated for these routes of administration. However, CYP2A6 expression in the lung was implemented according to the PK-Sim[®] expression database, to cover potential differences in cotinine formation [58]. Variability in predictions for most intravenous, oral, and transdermal studies is better covered compared with pulmonary studies, where the variability observed is higher than predicted. This is as expected because variability in model predictions results from physiological differences, while the high variability after smoking results from differences in puffing behavior (such as puff volumes) called smoking topography [59].

As a result, our findings support the assumption that differences in smoking topography also lead to differences in nicotine plasma concentrations [46, 60]. The fact that the model is able to describe nicotine PK after the use of combustible cigarettes and e-cigarettes with the same pulmonary administration model supports recent findings that

differences in plasma PK result from different smoking and vaping patterns, respectively [61].

Although transmucosal absorption was neglected during the administration of nicotine gums, predictions for nicotine plasma profiles show very promising results. The future development of a physiological transmucosal PBPK model could help predict cotinine metabolite concentrations after the administration of nicotine gums. The expansion of our PBPK model with a two-compartment transdermal skin model led to better descriptions of nicotine and cotinine metabolite plasma profiles after transdermal absorption, compared with an existing transdermal nicotine PBPK model [53]. Thereby, it was possible to extrapolate patch parameter sets from the 30-mg single-dose Bannon et al. [62] study to 15-mg and 60-mg patches and to a multiple-dose administration. This indicates that extrapolation from one dose to higher and lower doses as well as from single to multiple doses is possible with the implemented transdermal model. However, more research needs to be conducted to increase the mechanistic component of the transdermal model. As a result of the good predictive PK performance of the intravenous nicotine PBPK model, future studies could use the mechanistic model to de novo predict nicotine and cotinine plasma concentrations based on patch characteristics and in vitro dissolution data.

The simulation study results of nicotine brain concentration patterns show decisive differences: the lower dose nicotine gums (2 mg) yield lower brain concentrations of about half the magnitude ($C_{\max, \text{brain}}$) and extent (AUC_{brain}) as the cigarette study arm does. Brain concentrations during nicotine patch application also do not reach the same magnitude as the simulation with cigarettes does. In contrast, the use of 16 nicotine gums of 4 mg causes similar $C_{\max, \text{brain}}$ and AUC_{brain} values in brain concentrations. However, the fluctuation (peak-trough difference) stays lower, compared with smoking cigarettes. While the AUC_{brain} of the nicotine patch trails behind the AUC_{brain} of the cigarette study arm after 16 h, the AUC_{brain} during the last 8 h is larger, compared with inhalation.

The nicotine brain concentration data used for model building represent nicotine concentrations in the whole brain tissue and do not specifically show concentrations at the nicotine receptor site. Thus, brain concentration simulations were also executed for brain tissue concentrations. To describe the brain tissue concentration profile included in the model development, the implementation of an influx and an efflux transporter in the BBB was necessary and is supported by the literature [21]. As data on nicotine brain tissue concentrations are scarce, only one brain kinetic profile was available to inform the model. Moreover, the brain tissue concentrations were determined only during a time span of 10 min after a single puff of combustible cigarettes [11]. Therefore, extrapolations to brain tissue

simulations, especially of higher doses and longer time-frames, have to be interpreted carefully.

The magnitude of increase in heart rate is a surrogate measure for general pharmacological actions of nicotine. Two PBPK/PD heart rate models from the literature included studies only after intravenous and transdermal administration of nicotine [52, 53]. In contrast, while our PD model was also built based on intravenous administration data, it was expanded and evaluated with heart rate data from study participants consuming combustible cigarettes, e-cigarettes, and nicotine gums. Moreover, we included circadian rhythm for heart rate, as the heart rate undergoes marked fluctuations throughout the day [63]. We succeeded in incorporating acute tolerance development to the heart rate effect, which can not only be observed after the intake of nicotine but also after other substances, such as cocaine or ponesimod [20, 64]. Unfortunately, no heart rate data measured during a whole day of nicotine administration were available. The longest study which is included in the PD model development lasted about 6 h. Hence, extrapolations beyond this time domain should be investigated carefully.

The positive chronotropic effect of nicotine probably results from several effects. First, nicotine stimulates epinephrine and norepinephrine release by the activation of the ligand-gated cation channel nicotine acetylcholine receptors localized mainly on peripheral postganglionic sympathetic nerve endings and the adrenal medulla. Additionally, sympathetic stimulation can occur through the activation of peripheral carotid body chemoreceptors [65–67]. Moreover, a close relationship between plasma concentrations of nicotine and the cardiovascular effects has been observed after acute exposure to nicotine [9, 65]. As a result, the PD effect was linked to the plasma concentrations. Linking the PD effect to concentrations of the heart or the brain compartment led to less precise predictions of heart rate changes.

Simulations of heart rate changes during the administration of four cigarettes, 16 cigarettes (1.4 mg each, smoked within 8 h), 16 nicotine gums (2 mg each), and a transdermal nicotine patch (21 mg in 24 h) have been performed (see Sect. 3.12 of the ESM). The results suggest a persistent increase in the baseline heart rate when smoking one cigarette every 30 min (about 9 beats/min), which is supported by clinical studies [67]. Whereas only a slight increase of heart rate baseline can be observed when simulating the administration of cigarettes smoked 2 h apart, an increased baseline level holds true also for the administration of nicotine gums and the nicotine patch, albeit to a lower extent (about 6 beats/min and 4 beats/min, respectively). These differences are consistent with published work showing a decrease in heart rate when switching from smoking cigarettes to the use of nicotine gums or patches [68, 69].

5 Conclusions

A comprehensive whole-body parent–metabolite PBPK/PD model of nicotine and cotinine has been built that can predict (1) nicotine and cotinine plasma concentration–time profiles after various routes of administration, (2) nicotine brain tissue concentrations, and (3) the positive chronotropic effect of nicotine. The physiologically based modeling approach integrated the available *in vitro*, *in vivo*, and *in silico* information on nicotine and could help enhance the understanding of dependence on combustible cigarettes and e-cigarettes. The model was used to simulate and compare nicotine brain concentration patterns during smoking and the application of NRTs. The model is thoroughly documented in the ESM, and the model files are publicly available in the OSP repository (<https://www.open-systems-pharmacology.org>). With that, the model can be used for the development of a detailed physiological transdermal and transmucosal nicotine model, contribute to a library of PBPK models for predictions in special populations, and help with future investigations of nicotine pharmacokinetics and pharmacodynamics, including the design of clinical trials and novel formulations to treat nicotine dependence.

Acknowledgement Open Access funding provided by Projekt DEAL.

Compliance with Ethical Standards

Funding This project has received funding from the German Federal Ministry of Education and Research (BMBF), 031L0153, “Alternativmethoden zum Tierversuch” and 03XP0196, “NanoCare4.0 - Anwendungssichere Materialinnovationen”. Data used for model development were collected in part with the support of grants DA039264 and DA012393 from the National Institute on Drug Abuse, USA.

Conflict of interest Neal Benowitz has been a consultant to Pfizer and Achieve Life Sciences, companies that market or are developing smoking cessation medications. He has also been a paid witness in litigation against tobacco companies. Lukas Kovar, Dominik Selzer, Hannah Britz, Gideon St.Helen, Yvonne Kohl, Robert Bals, and Thorsten Lehr have no conflicts of interest that are directly relevant to the content of this article.

Open Access This article is licensed under a Creative Commons Attribution-NonCommercial 4.0 International License, which permits any non-commercial use, sharing, adaptation, distribution and reproduction in any medium or format, as long as you give appropriate credit to the original author(s) and the source, provide a link to the Creative Commons licence, and indicate if changes were made. The images or other third party material in this article are included in the article’s Creative Commons licence, unless indicated otherwise in a credit line to the material. If material is not included in the article’s Creative Commons licence and your intended use is not permitted by statutory regulation or exceeds the permitted use, you will need to obtain permission directly from the copyright holder. To view a copy of this licence, visit <http://creativecommons.org/licenses/by-nc/4.0/>.

References

1. World Health Organization. WHO report on the global tobacco epidemic, 2019. Geneva: World Health Organization; 2019. Licence: CC BY-NC-SA 3.0 IGO.
2. World Lung Foundation. The tobacco atlas. 5. Atlanta: American Cancer Society; 2015.
3. Benowitz NL. Nicotine addiction. *N Engl J Med*. 2010;362:2295–303.
4. Remarks prepared for testimony before a U.S. House Energy and Commerce Subcommittee on FDA Regulation of Electronic Nicotine Delivery Systems and Investigation of Vaping Illnesses, Acting Commissioner of Food and Drugs, Norman E. “Ned” Sharpless. 2019. <https://www.fda.gov/news-events/press-announcements/remarks-prepared-testimony-us-house-energy-and-commerce-subcommittee-fda-regulation-electronic>. Accessed 14 Oct 2019.
5. Bhatnagar A, Payne TJ, Robertson RM. Is there a role for electronic cigarettes in tobacco cessation? *J Am Heart Assoc*. 2019;8:e012742.
6. Benowitz NL. Pharmacology of nicotine: addiction, smoking-induced disease, and therapeutics. *Annu Rev Pharmacol Toxicol*. 2009;49:57–71.
7. Batra A, Klingler K, Landfeldt B, Friederich HM, Westin A, Danielsson T. Smoking reduction treatment with 4-mg nicotine gum: a double-blind, randomized, placebo-controlled study. *Clin Pharmacol Ther*. 2005;78:689–96.
8. Hays JT, Croghan IT, Schroeder DR, Offord KP, Hurt RD, Wolter TD, et al. Over-the-counter nicotine patch therapy for smoking cessation: results from randomized, double-blind, placebo-controlled, and open label trials. *Am J Public Health*. 1999;89:1701–7.
9. Benowitz NL, Porchet H, Sheiner L, Jacob P. Nicotine absorption and cardiovascular effects with smokeless tobacco use: comparison with cigarettes and nicotine gum. *Clin Pharmacol Ther*. 1988;44:23–8.
10. Benowitz NL, Chan K, Denaro CP, Jacob P. Stable isotope method for studying transdermal drug absorption: the nicotine patch. *Clin Pharmacol Ther*. 1991;50:286–93.
11. Rose JE, Mukhin AG, Lokitz SJ, Turkington TG, Herskovic J, Behm FM, et al. Kinetics of brain nicotine accumulation in dependent and nondependent smokers assessed with PET and cigarettes containing ¹¹C-nicotine. *Proc Natl Acad Sci USA*. 2010;107:5190–5.
12. Xian H, Scherrer JF, Madden PAF, Lyons MJ, Tsuang M, True WR, et al. The heritability of failed smoking cessation and nicotine withdrawal in twins who smoked and attempted to quit. *Nicotine Tob Res*. 2003;5:245–54.
13. Heitjan DF, Asch DA, Ray R, Rukstalis M, Patterson F, Lerman C. Cost-effectiveness of pharmacogenetic testing to tailor smoking-cessation treatment. *Pharmacogenom J*. 2008;8:391–9.
14. Lerman C, Schnoll RA, Hawk LW, Cinciripini P, George TP, Wileyto EP, et al. Use of the nicotine metabolite ratio as a genetically informed biomarker of response to nicotine patch or varenicline for smoking cessation: a randomised, double-blind placebo-controlled trial. *Lancet Respir Med*. 2015;3:131–8.
15. Hukkanen J, Jacob P, Benowitz NL. Metabolism and disposition kinetics of nicotine. *Pharmacol Rev*. 2005;57:79–115.
16. Mroziewicz M, Tyndale RF. Pharmacogenetics: a tool for identifying genetic factors in drug dependence and response to treatment. *Addict Sci Clin Pract*. 2010;5:17–29.
17. Benowitz NL. Cigarette smoking and cardiovascular disease: pathophysiology and implications for treatment. *Prog Cardiovasc Dis*. 2003;46:91–111.

18. Benowitz NL, Dains KM, Dempsey D, Yu L, Jacob P. Estimation of nicotine dose after low-level exposure using plasma and urine nicotine metabolites. *Cancer Epidemiol Biomark Prev.* 2010;19:1160–6.
19. Zhao P, Zhang L, Grillo JA, Liu Q, Bullock JM, Moon YJ, et al. Applications of physiologically based pharmacokinetic (PBPK) modeling and simulation during regulatory review. *Clin Pharmacol Ther.* 2011;89:259–67.
20. Lott D, Lehr T, Dingemans J, Krause A. Modeling tolerance development for the effect on heart rate of the selective $5\text{-HT}_1\text{A}$ receptor modulator ponesimod. *Clin Pharmacol Ther.* 2018;103:1083–92.
21. Tega Y, Yamazaki Y, Akanuma S, Kubo Y, Hosoya K. Impact of nicotine transport across the blood-brain barrier: carrier-mediated transport of nicotine and interaction with central nervous system drugs. *Biol Pharm Bull.* 2018;41:1330–6.
22. Benowitz NL, Jacob P. Metabolism of nicotine to cotinine studied by a dual stable isotope method. *Clin Pharmacol Ther.* 1994;56:483–93.
23. Gubner NR, Kozar-Konieczna A, Szoltysek-Boldys I, Slodczyk-Mankowska E, Goniewicz J, Sobczak A, et al. Cessation of alcohol consumption decreases rate of nicotine metabolism in male alcohol-dependent smokers. *Drug Alcohol Depend.* 2016;163:157–64.
24. De Schepper PJ, Van Hecken A, Daenens P, Van Rossum JM. Kinetics of cotinine after oral and intravenous administration to man. *Eur J Clin Pharmacol.* 1987;31:583–8.
25. Benowitz NL, Jacob P. Nicotine and cotinine elimination pharmacokinetics in smokers and nonsmokers. *Clin Pharmacol Ther.* 1993;53:316–23.
26. Simon DL, Iglauer A. The acute effect of chewing tobacco and smoking in habitual users. *Ann N Y Acad Sci.* 1960;90:119–32.
27. Porchet HC, Benowitz NL, Sheiner LB. Pharmacodynamic model of tolerance: application to nicotine. *J Pharmacol Exp Ther.* 1988;244:231–6.
28. Morjaria Y, Irwin WJ, Barnett PX, Chan RS, Conway BR. In vitro release of nicotine from chewing gum formulations. *Dissolution Technol.* 2004;11:12–5.
29. Houseman TH. Studies of cigarette smoke transfer using radioisotopically labelled tobacco constituents part II: the transference of radioisotopically labelled nicotine to cigarette smoke. *Beitrag zur Tab Int Contrib to Tob Res.* 1973;7:142–7.
30. Wishart DS, Knox C, Guo AC, Shrivastava S, Hassanali M, Stothard P, et al. DrugBank: a comprehensive resource for in silico drug discovery and exploration. *Nucleic Acids Res.* 2006;34:D668–72.
31. Nielsen HM, Rassing MR. Nicotine permeability across the buccal TR146 cell culture model and porcine buccal mucosa in vitro: effect of pH and concentration. *Eur J Pharm Sci.* 2002;16:151–7.
32. Alharbi O, Xu Y, Goodacre R. Simultaneous multiplexed quantification of nicotine and its metabolites using surface enhanced Raman scattering. *Analyst.* 2014;139:4820–7.
33. Zissimos AM, Abraham MH, Barker MC, Box KJ, Tam KY. Calculation of Abraham descriptors from solvent-water partition coefficients in four different systems; evaluation of different methods of calculation. *J Chem Soc Perkin Trans.* 2002;2:470–7.
34. Svensson CK. Clinical pharmacokinetics of nicotine. *Clin Pharmacokinet.* 1987;12:30–40.
35. Benowitz NL, Kuyt F, Jacob P, Jones RT, Osman AL. Cotinine disposition and effects. *Clin Pharmacol Ther.* 1983;34:604–11.
36. Yamazaki H, Inoue K, Hashimoto M, Shimada T. Roles of CYP2A6 and CYP2B6 in nicotine C-oxidation by human liver microsomes. *Arch Toxicol.* 1999;73:65–70.
37. Fukami T, Nakajima M, Yoshida R, Tsuchiya Y, Fujiki Y, Katoh M, et al. A novel polymorphism of human CYP2A6 gene CYP2A6*17 has an amino acid substitution (V365M) that decreases enzymatic activity in vitro and in vivo. *Clin Pharmacol Ther.* 2004;76:519–27.
38. Hosono H, Kumondai M, Maekawa M, Yamaguchi H, Mano N, Oda A, et al. Functional characterization of 34 CYP2A6 allelic variants by assessment of nicotine C-oxidation and coumarin 7-hydroxylation activities. *Drug Metab Dispos.* 2017;45:279–85.
39. Murphy SE, Raulinaitis V, Brown KM. Nicotine 5'-oxidation and methyl oxidation by P450 2A enzymes. *Drug Metab Dispos.* 2005;33:1166–73.
40. Xu C, Rao YS, Xu B, Hoffmann E, Jones J, Sellers EM, et al. An in vivo pilot study characterizing the new CYP2A6*7, *8, and *10 alleles. *Biochem Biophys Res Commun.* 2002;290:318–24.
41. Dicke KE, Skrlin SM, Murphy SE. Nicotine and 4-(methylnitrosamino)-1-(3-pyridyl)-butanone metabolism by cytochrome P450 2B6. *Drug Metab Dispos.* 2005;33:1760–4.
42. Rodgers T, Rowland M. Mechanistic approaches to volume of distribution predictions: understanding the processes. *Pharm Res.* 2007;24:918–33.
43. Rodgers T, Leahy D, Rowland M. Physiologically based pharmacokinetic modeling I: predicting the tissue distribution of moderate-to-strong bases. *J Pharm Sci.* 2005;94:1259–76.
44. Rodgers T, Rowland M. Physiologically-based pharmacokinetic modeling 2: predicting the tissue distribution of acids, very weak bases, neutrals and zwitterions. *J Pharm Sci.* 2006;95:1238–57.
45. Hindmarsh AC, Reynolds DR, Serban R, Woodward CS, Gardner DJ, Cohen SD, et al. Open systems pharmacology suite manual, version 7.4.; 2018.
46. Armitage AK, Dollery CT, George CF, Houseman TH, Lewis PJ, Turner DM. Absorption and metabolism of nicotine from cigarettes. *Br Med J.* 1975;4:313–6.
47. Hammond D, Fong GT, Cummings KM, O'Connor RJ, Giovino GA, McNeill A. Cigarette yields and human exposure: a comparison of alternative testing regimens. *Cancer Epidemiol Biomark Prev.* 2006;15:1495–501.
48. Benowitz NL. Compensatory smoking of low-yield cigarettes. In: Burns DM, Benowitz NL, Amacher RH (eds) *Smok Tob Control Monogr No 13.* 2001: p. 39–64.
49. Robinson DE, Balter NJ, Schwartz SL. A physiologically based pharmacokinetic model for nicotine and cotinine in man. *J Pharmacokinet Biopharm.* 1992;20:591–609.
50. Plowchalk DR, Andersen ME, DeBethizy JD. A physiologically based pharmacokinetic model for nicotine disposition in the Sprague-Dawley rat. *Toxicol Appl Pharmacol.* 1992;116:177–88.
51. Yamazaki H, Horiuchi K, Takano R, Nagano T, Shimizu M, Kitajima M, et al. Human blood concentrations of cotinine, a bio-monitoring marker for tobacco smoke, extrapolated from nicotine metabolism in rats and humans and physiologically based pharmacokinetic modeling. *Int J Environ Res Public Health.* 2010;7:3406–21.
52. Teeguarden JG, Housand CJ, Smith JN, Hinderliter PM, Gunawan R, Timchalk CA. A multi-route model of nicotine-cotinine pharmacokinetics, pharmacodynamics and brain nicotinic acetylcholine receptor binding in humans. *Regul Toxicol Pharmacol.* 2013;65:12–28.
53. Gajewska M, Worth A, Urani C, Briesen H, Schramm K-W. The acute effects of daily nicotine intake on heart rate—a toxicokinetic and toxicodynamic modelling study. *Regul Toxicol Pharmacol.* 2014;70:312–24.
54. Zanger UM, Klein K, Saussele T, Bliedernicht J, Hofmann MH, Schwab M. Polymorphic CYP2B6: molecular mechanisms and emerging clinical significance. *Pharmacogenomics.* 2007;8:743–59.
55. Eichelbaum M, Ingelman-Sundberg M, Evans WE. Pharmacogenomics and individualized drug therapy. *Annu Rev Med.* 2006;57:119–37.

56. Kovar L, Schmidt S, Derendorf H. Maßgeschneidert: Die Pharmakogenetik ebnet den Weg für erfolgreiche individualisierte Interventionen. *DAZ*; 2018. p. 3000–4.
57. Cullen KA, Ambrose BK, Gentzke AS, Apelberg BJ, Jamal A, King BA. Use of electronic cigarettes and any tobacco product among middle and high school students: United States, 2011–2018. *Am J Public Health*. 2018;67:1277.
58. Meyer M, Schneckener S, Ludewig B, Kuepfer L, Lippert J. Using expression data for quantification of active processes in PBPK modeling. *Drug Metab Dispos*. 2012;40:892–901.
59. Schorp MK. Summary of literature data on smoking topography. In: Pick W, Houlgate P, Schorp MK, et al. (eds) *A Rev Hum Smok Behav Recomm a New ISO Stand Mach Smok Cigarettes*; Rep Ad Hoc WG9 Smok R Beirut, Lebanon Am Univ Beirut. 2005: p. 28–50.
60. Ross KC, Dempsey DA, St. Helen G, Delucchi K, Benowitz NL. The influence of puff characteristics, nicotine dependence, and rate of nicotine metabolism on daily nicotine exposure in African American smokers. *Cancer Epidemiol Biomark Prev*. 2016;25:936–43.
61. St Helen G, Ross KC, Dempsey DA, Havel CM, Jacob P, Benowitz NL. Nicotine delivery and vaping behavior during ad libitum E-cigarette access. *Tob Regul Sci*. 2016;2:363–76.
62. Bannon YB, Corish J, Corrigan OI, Devane JG, Kavanagh M, Mulligan S. Transdermal delivery of nicotine in normal human volunteers: a single dose and multiple dose study. *Eur J Clin Pharmacol*. 1989;37:285–90.
63. Vandewalle G, Middleton B, Rajaratnam SMW, Stone BM, Thorleifsdottir B, Arendt J, et al. Robust circadian rhythm in heart rate and its variability: influence of exogenous melatonin and photoperiod. *J Sleep Res*. 2007;16:148–55.
64. Ambre JJ, Belknap SM, Nelson J, Ruo TI, Shin SG, Atkinson AJ. Acute tolerance to cocaine in humans. *Clin Pharmacol Ther*. 1988;44:1–8.
65. Haass M, Kübler W. Nicotine and sympathetic neurotransmission. *Cardiovasc Drugs Ther*. 1996;10:657–65.
66. Stéphan-Blanchard E, Bach V, Telliez F, Chardon K. Perinatal nicotine/smoking exposure and carotid chemoreceptors during development. *Respir Physiol Neurobiol*. 2013;185:110–9.
67. Benowitz NL, Gourlay SG. Cardiovascular toxicity of nicotine: implications for nicotine replacement therapy. *J Am Coll Cardiol*. 1997;29:1422–31.
68. Fagerström KO, Schneider NG, Lunell E. Effectiveness of nicotine patch and nicotine gum as individual versus combined treatments for tobacco withdrawal symptoms. *Psychopharmacology*. 1993;111:271–7.
69. Stein PK, Rottman JN, Kleiger RE. Effect of 21 mg transdermal nicotine patches and smoking cessation on heart rate variability. *Am J Cardiol*. 1996;77:701–5.
70. Mendelson JH, Goletiani N, Sholar MB, Siegel AJ, Mello NK. Effects of smoking successive low- and high-nicotine cigarettes on hypothalamic-pituitary-adrenal axis hormones and mood in men. *Neuropsychopharmacology*. 2008;33:749–60.
71. Benowitz NL, Kuyt F, Jacob P. Circadian blood nicotine concentrations during cigarette smoking. *Clin Pharmacol Ther*. 1982;32:758–64.
72. Feyerabend C, Ings RM, Russel MA. Nicotine pharmacokinetics and its application to intake from smoking. *Br J Clin Pharmacol*. 1985;19:239–47.
73. St Helen G, Nardone N, Addo N, Dempsey D, Havel C, Jacob P BN. Differences in nicotine intake and effects from electronic and combustible cigarettes among dual users. *Addiction*. 2019. <https://doi.org/10.1111/add.14884>. [Epub ahead of print].
74. Zevin S, Jacob P, Benowitz N. Cotinine effects on nicotine metabolism. *Clin Pharmacol Ther*. 1997;61:649–54.
75. Curvall M, Elwin CE, Kazemi-Vala E, Warholm C, Enzell CR. The pharmacokinetics of cotinine in plasma and saliva from non-smoking healthy volunteers. *Eur J Clin Pharmacol*. 1990;38:281–7.
76. Benowitz NL, Jacob P, Fong I, Gupta S. Nicotine metabolic profile in man: comparison of cigarette smoking and transdermal nicotine. *J Pharmacol Exp Ther*. 1994;268:296–303.
77. Du D. A single-dose, crossover-design bioequivalence study comparing two nicotine gum formulations in healthy subjects. *Adv Ther*. 2018;35:1169–80.
78. Dautzenberg B, Nides M, Kienzler J-L, Callens A. Pharmacokinetics, safety and efficacy from randomized controlled trials of 1 and 2 mg nicotine bitartrate lozenges (Nicotinell). *BMC Clin Pharmacol*. 2007;7:11.
79. Gupta SK, Benowitz NL, Jacob P, Rolf CN, Gorsline J. Bioavailability and absorption kinetics of nicotine following application of a transdermal system. *Br J Clin Pharmacol*. 1993;36:221–7.
80. Gilbert DG, Robinson JH, Chamberlin CL, Spielberger CD. Effects of smoking/nicotine on anxiety, heart rate, and lateralization of EEG during a stressful movie. *Psychophysiology*. 1989;26:311–20.
81. St Helen G, Havel C, Dempsey DA, Jacob P, Benowitz NL. Nicotine delivery, retention and pharmacokinetics from various electronic cigarettes. *Addiction*. 2016;111:535–44.